IOSR Journal of Applied Physics (IOSR-JAP)
e-ISSN: 2278-4861.Volume 8, Issue 1 Ver. I (Jan. - Feb. 2016), PP 38-46
www.iosrjournals

Improving the Estimation of Crop of Rice Using Higher Resolution Simulated Landsat Images

S.M. Ali[1,] S.S. Salman[2]

[1&2] *University of Baghdad, Iraq, Baghdad, Al- Jaderyia College of Science, Department of Remote Sensing*
[2] *College of Pharmacy*

Abstract: *Preferable estimate to the amount of agricultural yield is performed by using high-resolution satellite images. Unfortunately free available satellite images provide by the* ***Earth Resources and Science Center (EROS)*** *are either of low or moderate resolutions. For example the available Landsat satellite images are of 30meter/pixel resolution. Accordingly, analysis capability of such images may not be accurate because of the overlapping between the specifications of land cover components. This paper presents a method to estimate the areas of crop of rice by using Landsat images based on normalized difference vegetation Index (NDVI) and scatterplot classification methods (SCP). The crop of rice estimation is implemented on Landsat-8 (Operational Land Imager OLI) images. The OLI bands are enlarged by employing the discrete wavelet transform DWT method. The histograms of the enlarged higher resolution bands are pushed to match the histogram of its corresponding original multispectral bands by utilizing the histogram-specification method. The rice vegetate areas are then estimated by utilizing the NDVI and SCP methods from the original, wave enlarged, and enlarged-histogram-specified bands. To ensure the validation of the adopted method, the estimated areas are then compared with the real cultivated areas obtained from the Iraqi Ministry of Agriculture publications.*

Keywords: *Rice estimation areas, Normalized vegetation indices, Scatterplot classification, Discrete wavelet transformation, Histogram specification.*

I. Introduction

Rice is one of the most important agriculture crops in many countries. It is a primary food source for more than three billions of people worldwide. Forecasting rice yield before harvest is crucial, especially in regions characterized by climatic uncertainties. It enables planners and decision makers to deduce how much to import in the case of a shortfall or, optionally, to export in the case of a surplus. Forecasting also allows governments to develop a strategic contingency plans for distribution the food during times of famine. Therefore, monitoring the growth and development of plants with guesses of the production yield possess a great importance. Over the past twenty-five years, the multispectral images taken by satellites have proven as to be a powerful tool in determining the amounts of the productivity of agricultural crops. An important goal of agricultural remote sensing research is to spectrally estimate crop variables related to crop conditions, which can subsequently be entered into crop simulation and yield models [1-2]. The use of remote sensing is restricted by the cost and availability of fine resolution satellite images. It is natural that the high-resolution images have the ability to determine the amount of crops within the studied agricultural fields better than the moderate and low resolution images. But usually high-resolution images are sold at high prices. For example the cost per km^2 of newly acquired imagery is as follows; the ***Worldview-2*** (0.5m pan resolution) is about €30/km^2, the ***Ikonos*** (0.8-3m resolution) is about €25/km^2, and the high quality airborne LiDAR survey is in the order of €450/km^2 [https://earthobservation.wordpress.com]. In addition to high prices, the high resolution images do not cover large areas and does not include a wide range of multispectral bands.

Hence, we will try in our present search to create satellite images meets the conditions listed above (i.e. free of charge, of high resolution, and of temporal and multispectral bands). The main source provides free temporal and multispectral Landsat band is the ***USGS Global Visualization Viewer of the Earth Resources and Science Center (EROS)*** [http://glovis.usgs.gov/]. Image resolution enhancement techniques based on replacement of discrete wavelet transform (DWT) high frequency subbands (i.e. LH, HL, and HH) by the high frequency of stationary wavelet transform (SWT) subbands and using input image instead of low frequency DWT subband will be used to produce higher resolution image as an output of inverse discrete wavelet (IDWT) process [3]. To achieve the greatest match between the simulated and original images, histogram specification (or matching) method will be applied [4]. For the purpose of verification of the quality of the simulated images we will try to account the rice cultivated in the study area and compare them with the real data released by the Iraqi Ministry of Agriculture. Two types of estimation of cultivated area will be tried; applying the NDVI [5], and scatterplot classification [6].

II. Study Area

The investigations were performed in ***Al-Najaf and Al-Qadisiya*** provinces in the middle-south of Iraq, at 32.216°→31.550°N latitude, and 44.161°→ 44.724°E longitude, as shown in Fig. 1. The study areas have been selected because they represent the central area for rice production in Iraq. They represent a fertile mudslides land area, about 30km south of **Najaf province**, 230 km southwest of the **Baghdad** (capital of Iraq). A river (called **Al-Hidia**) of length 25km, which is part of the **Euphrates River**, passes through them. The study area is surrounded by rice plantations and palm groves.

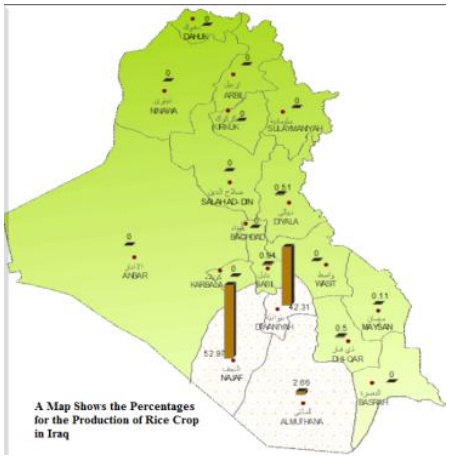

Iraq Map shows the percentage for the Production of Rice Crop in Iraqi provinces.

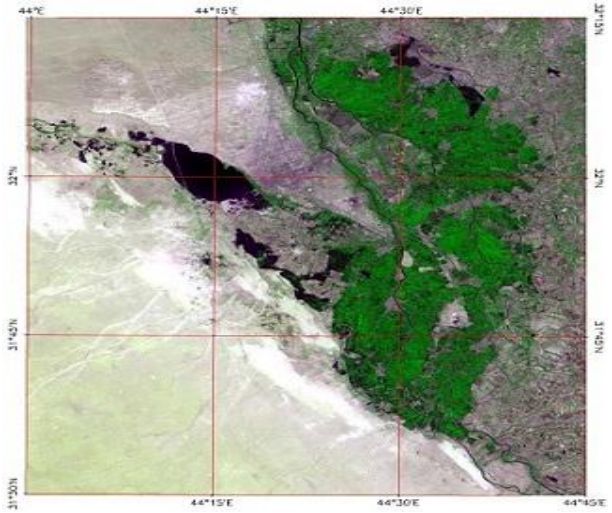

Photomap of the study area Al-Najaf and Al-Qadisiya districts

Fig.1: Administrative map of Iraq country and photomap of the study area

III. Rice Growing Stages

Rice is the principal meal in Iraq's kitchens; it comes in the second place after wheat. Its cultivation is concentrated in the central and southern regions of the country. In the province of Najaf (exclusively) the area planted with this crop on 1996 reached to about 67037 Hectares, its production reached to about 102.487 tons an average yield of about 1529.58 kg/Hectares. Typically, rice cultivation begins in the study area (Najaf province) in mid-June and up to the top of the vegetative phase after 3 to 3.5 months (i.e. between September and October), then up to the harvest stage in thirty days (i.e. November), as illustrated in Fig. 2.

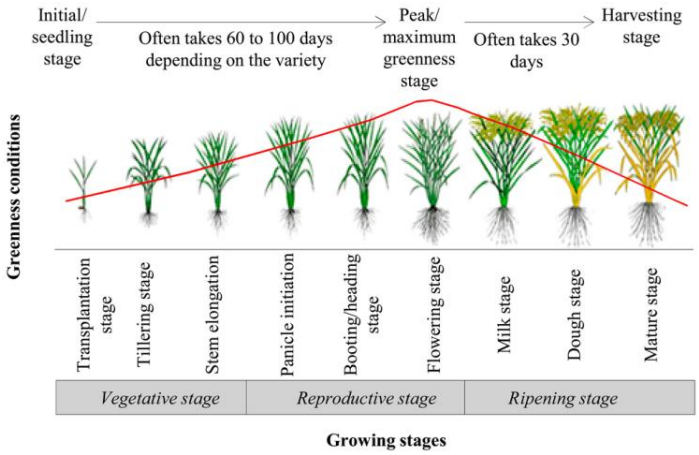

Fig.2: Illustrates the growing stages of the rice crop [7].

For the above mentioned reason, the selected Landsat-8 (OLI) bands, shown in Fig.3, were on September (i.e. maximum greenness stage) to achieve best estimation of the cultivated area.

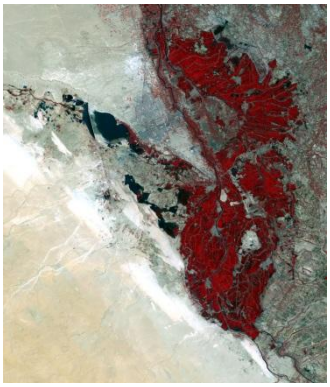

(a) Colored OLI Combination Bands

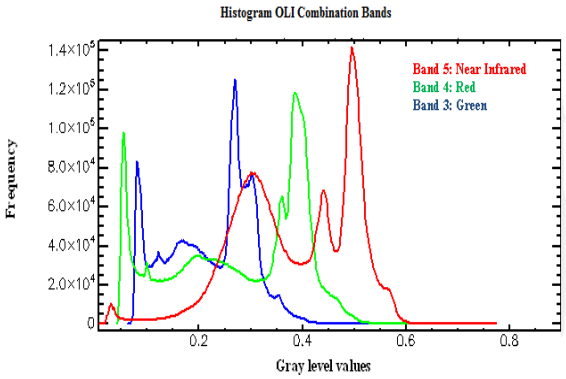

(b)

Fig.3: OLI colored image (size 2382×2786 pixels, spatial resolution 30m), color combination (Near-Infrared, Red, and Green in RGB coloring mode), acquired at 2013-9-28, (b) It histogram

IV. Enhancement Of Image Resolution By Using DWT And SWT Method

One of the commonly used techniques for image resolution enhancement is interpolation. Interpolation has been widely used in many image processing applications such as facial reconstruction, multiple description coding, and super resolution. There are three well known interpolation techniques, namely nearest neighbor interpolation, bilinear interpolation, and bicubic interpolation [3]. Image resolution enhancement in the wavelet domain is a relatively new topic proposed in [8]. Discrete wavelet transform (DWT) [9] is a wavelet transforms used in image processing. It decomposes an image into different subband images, namely low-low (LL), low-High (LH), High-Low (HL), and High-High (HH). Another wavelet transform which has been used in several image processing applications is stationary wavelet transform (SWT) [10]. The SWT is similar to DWT but it does not use down-sampling, hence the subbands have the same size as the input image. Finally, the enhance resolution (Enlarge size) image can be obtained by implementing the discrete wavelet transform (IDWT) on the following subbands: original low resolution image (as LL subband), and the combination of the high frequency subbands (i.e. LH, HL, and HH) of the enlarged by factor $\uparrow^2$ of DWT+SWT, as illustrated in Fig.4. The output resolution enhanced (enlarged) images and their histograms are shown in Fig.5.

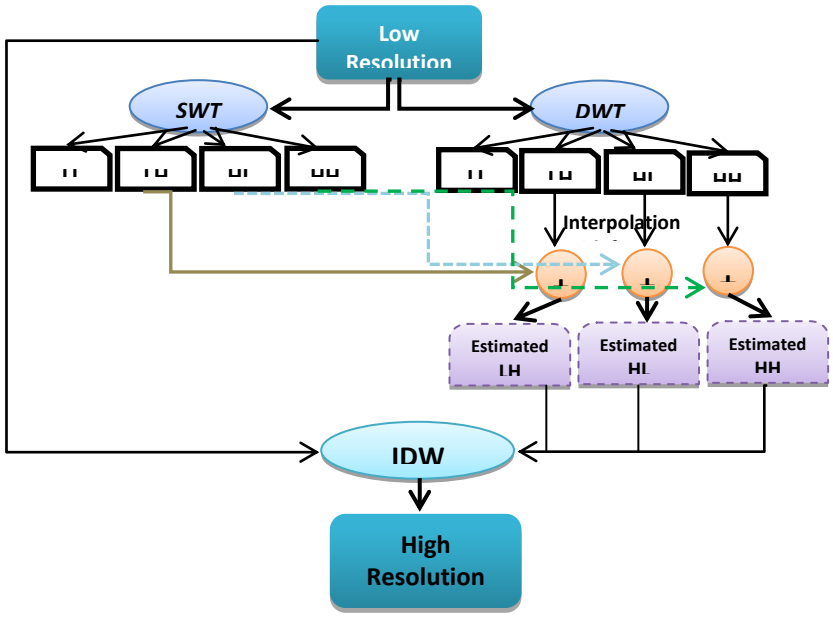

Fig.4: Block diagram of the image resolution enhancement algorithm [8].

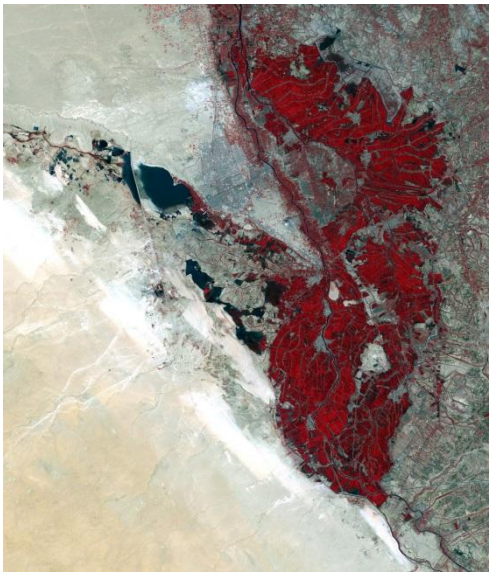

(a) Enhanced Resolution Colored OLI Combination Bands

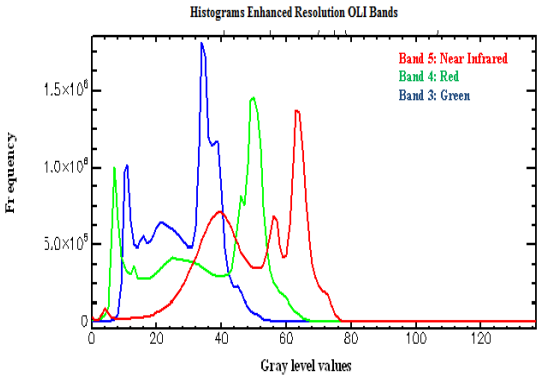

(b)

Fig.5: Enhanced resolution OLI colored image (size 4764×5572 pixels, spatial resolution 15m), color combination (Near-Infrared, Red, Green in RGB coloring mode), acquired at 2013-9-28, (b) It histogram

V. Histogram Specification Technique

Particularly, it is useful sometimes to be able to specify the shape of the histogram that is required to be used in a specific application; the method is called ***histogram matching*** or ***histogram specification*** [11]. Consider a continuous gray levels r (of probability *pr(r)*), and a continuous random variables z (of probability *pr(z)*). Let r and z denote the gray levels of the input and output (processed) images, respectively. We can estimate *pr(r)* from the given input image, while *pr(z)* is the specified probability density function "pdf" that we wish the output image to have. Let *s* be a random variable with the following property [10];

$$S = T(r) = \int_0^r \rho_r(w)\, dw \tag{1}$$

Where *w* is a dummy variable of integration.

Let us also define a random variable *z* with the property;

$$G(z) = \int_0^z \rho_z(t)\, dt = S \tag{2}$$

Where *t* is also a dummy variable of integration

It follows from these two above equations that *G{z) = T(r)* and, therefore, that *z* must satisfy the condition;

$$z = G^{-1}(s) = G^{-1}[T(r)] \tag{3}$$

The discrete formulations of the above equations are as follows

$$z_k = G^{-1}[T(r_k)] \qquad for \quad k = 0,1,2,....,L-1$$

and (4)

$$z_k = G^{-1}(s_k) \qquad for \quad k = 0,1,2,.....,L-1$$

Finally the discrete version of equation (3) is;

$$z_k = G^{-1}(s_k) = G^{-1}[T(r_k)] \qquad for \quad k = 0,1,2,.....,L-1 \tag{5}$$

Where:

$$s_k = T(r_k) = \sum_{j=0}^{k} \rho_r(r_j) = \sum_{j=0}^{k} \frac{n_j}{n} \qquad for \quad k = 0,1,2,...., L-1 \tag{6}$$

Where n is the total number of pixels in the image, n_j is the number of pixels with gray level r_j, and L is the number of discrete gray levels.

The specified histogram colored image of OLI bands are shown on Fig.6.

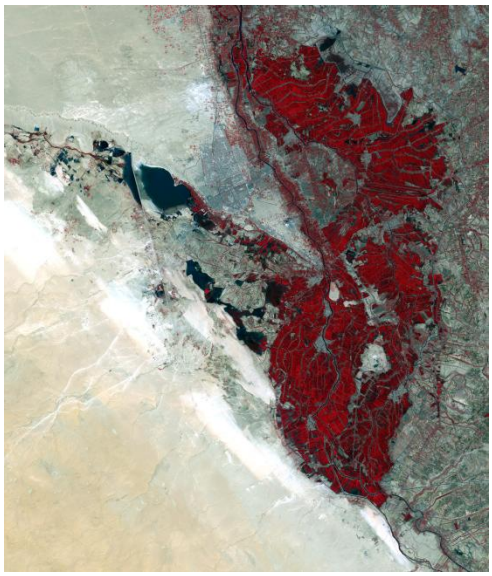

(a) Specified Histograms of Enhanced Resolution Colored OLI Combination Bands

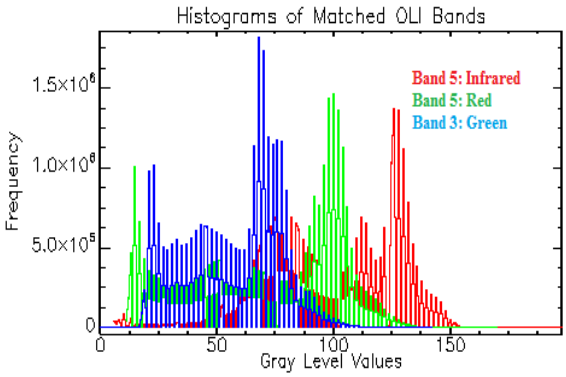

(b)

Fig.6: (a) Specified histograms of OLI bands shown in Fig.(5). (b) Their histograms.

The effect of histogram specification (matching) can be easily discovered by comparing their histograms with those shown in Figs.(3 and 5).

VI. Vegetation Indices

Remote sensing phenology studies use data gathered by satellite sensors that measure wavelengths of light absorbed and reflected by green plants. Certain pigment in plant leaves strongly absorb wavelengths of Visible Red (0.630 - 0.680 µm) light. The leaves themselves strongly reflect wavelengths of near-infrared (0.845 - 0.885 µm) light, which is invisible to human eyes. As a plant canopy changes from early spring growth to late season maturity and senescence, these reflectance properties also change. Vegetation indices are indicators used to describe the greenness, the relative density, and health of vegetation in satellite images. Although there are several vegetation indices, one of the most widely used is the *Normalized Difference Vegetation Index* (NDVI). Thus, NDVI was one of the most successful of many attempts to simply and quickly identify vegetated areas and their condition. It remains the most well-known and used index to detect live green plant canopies in multispectral remote sensing data. Mathematically, the NDVI is represented by [12];

$$NDVI = \frac{\rho_{NIR} - \rho_{RED}}{\rho_{NIR} + \rho_{RED}} \tag{7}$$

Where: ρ_{RED} and ρ_{NIR} represent, respectively, the visible red and near infrared reflectance.

The value of NDVI ranges from -1 to 1, the common range for green vegetation is 0.2 to 0.8, [13]. Areas of barren rock, sand, or snow usually show very low (e.g. 0.1 or less). Sparse vegetation such as shrubs and grasslands or senescing crops may result in moderate values (i.e. ~ 0.2 to 0.5). High NDVI values (~ 0.6 to 0.9) correspond to dense vegetation such as that found in temperate and tropical forests or crops at their peak growth stage, [14]. In this research, the NDVI values adopted to isolate dense vegetative was $0.4 \leq NDVI \leq 0.8$, as illustrated in Fig, **7.**

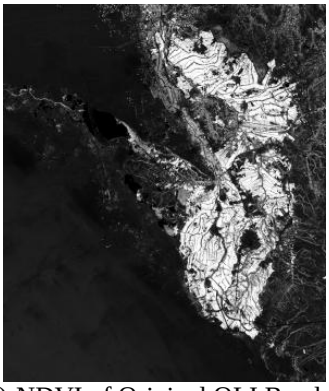

(a) NDVI of Original OLI Bands

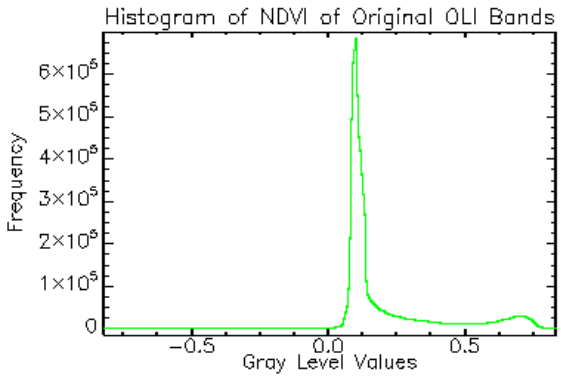

(b)

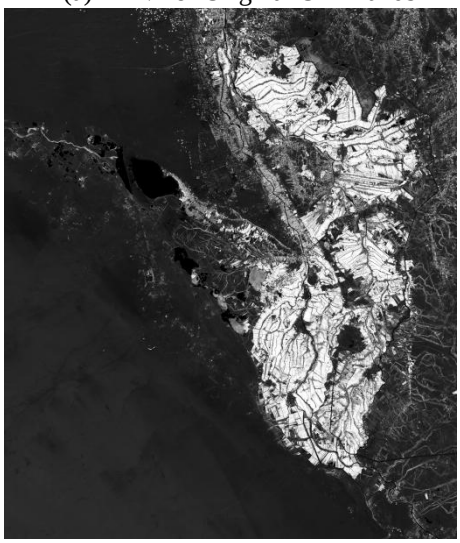

(a) NDVI of Enhanced Resolution OLI Bands

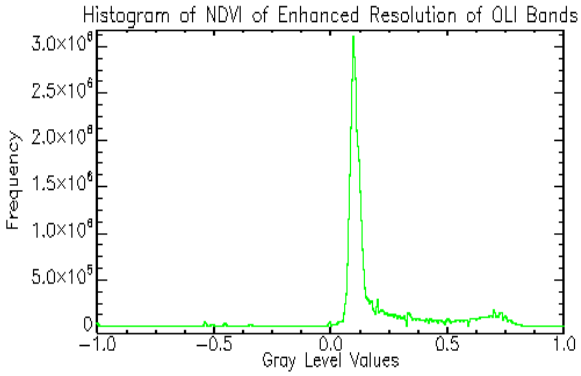

(b)

(a) NDVI of Enhanced Resolution and Histogram Specified OLI Bands

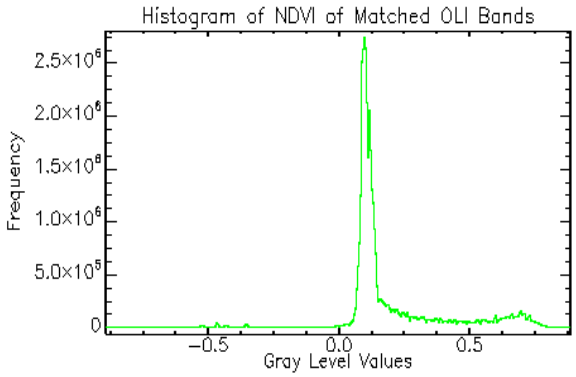

(b)

Fig.7: illustrates the NDVI images of original OLI bands and their Enhanced Resolution and Corrected Histograms Versions with their Histograms.

Table-1 shows the accuracy of the calculated acreage by using the NDVI techniques for different way and compared with the actual acreage for the years 2013 that have been obtained from the publications of the Iraqi Ministry of Agriculture; i.e. 90577Hectares.

TABLE-1 NDVI Estimation of Cultivated Areas

Data used	Percentage area	Predictive of Rice Cultivated Areas Hectares	Accuracy
Original Bands	14.2133%	84891	93.54%
Wavelet Resolution Enhanced Bands	14.1265%	84372	92.97%
Histogram Specified Bands of Resolution Enhanced Bands	14.3544 %	85733	94.47%

VII. Scatterplot Classification Method

It is well known that the soil has property which shows a linear relationship between "*NIR*" and "*Red*" reflectance bands. The length of the linearity responses of this relationship is affected by the soil's dryness or wetness contents; i.e. it is shortened for homogenous soils, and extended as the soil's contents varies. Therefore, as the soil line is defined, the corresponding reflectance regions of the other spectral classes (i.e. dry soil, wet soil, dry vegetation, wet vegetation, dense-healthy vegetation, and water areas) can be decided accordingly. These behaviors have been benefited by Ali [6] to introduce an automatic multispectral image classification based on scatterplot method. The method is based on dividing the scatterplot diagram of the Red and NIR bands into regions corresponding to the reflectance values of the Landcover components, as illustrated in Fig.8.

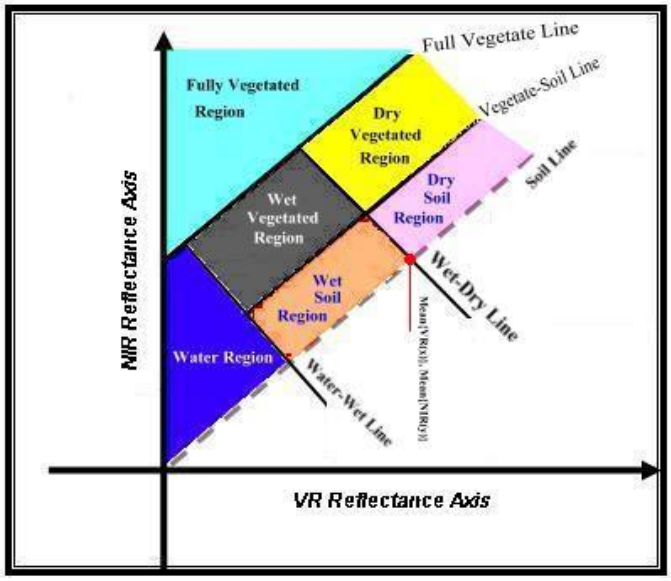

Fig.8: Classification Scheme Based on Scatterplot Method.

In this research, the scatterplot classification method will be adopted to predict the vegetated area in the images of the study area, as illustrated in Fig.9.

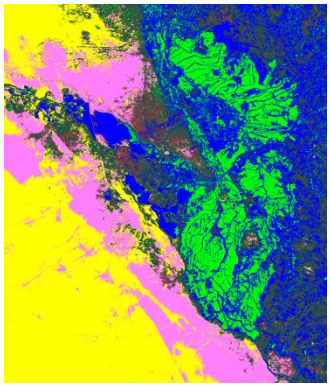

(a)Scatterplot Classification of Original OLI Bands

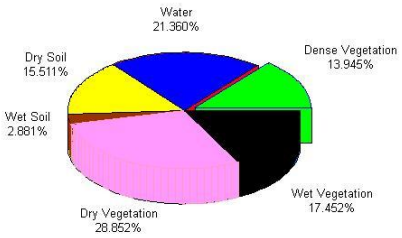

(b)Percentage classes of Original OLI Bands

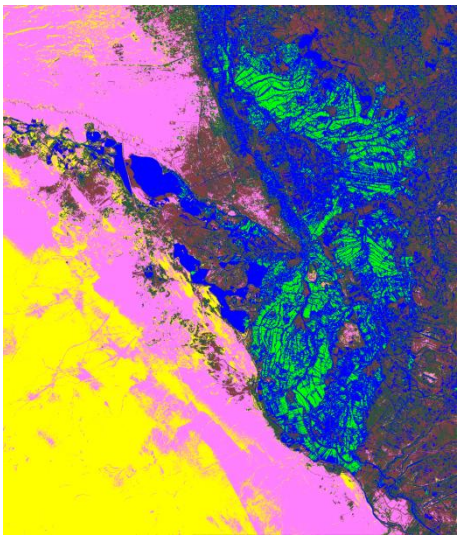

(c) Scatterplot Classification of Enhanced

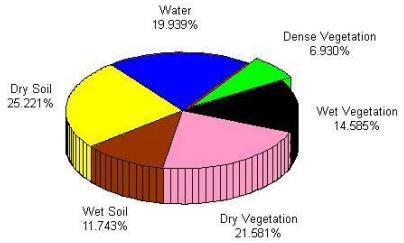

(d) Percentage classes of Enhanced

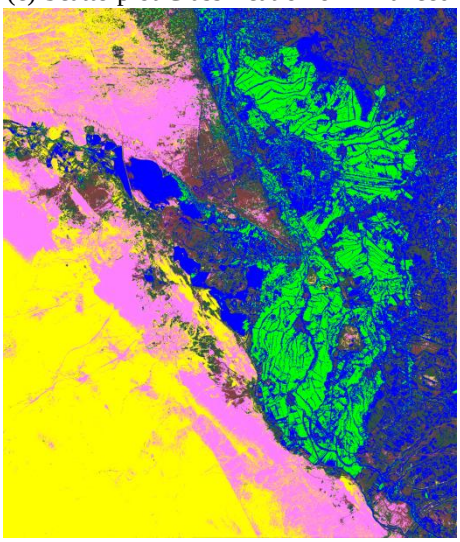

(e)Scatterplot Classification of Enhanced Resolution and Histogram Specified OLI Bands

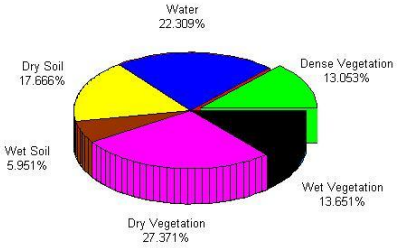

(f) Percentage classes of Enhanced Resolution and Histogram Specified OLI Bands

Fig.9: illustrates Scatterplot classification and Percentage classes images of original OLI bands and their Enhanced Resolution and Corrected Histograms Versions with their Histograms.

Table-2 shows the accuracy of the calculated acreage by using the Scatterplot classification techniques for different way and compared with the actual acreage for the years 2013 that have been obtained from the publications of the Iraqi Ministry of Agriculture; i.e. 90577Hectares. ..

TABLE-2 Scatterplot Estimation of Rice Cultivated Areas

Data used	Percentage area%	Predictive (Agriculture area) Hectares	Accuracy
Original	13.945%	83288	86.8%
Magnified Bands	6.930%	41392	43.1%
Magnified and Histogram Specified Bands	13.053%	77958	81.24%

VIII. Conclusions

Estimating the amount of productive of agricultural yields, using satellite images, is considered as an essential procedures followed by the developed countries to take prior precautions to provide a basket food to their citizens. To achieve acceptable results and compatible with the actual cultivated areas, the required satellite images should be characterized by high accuracy (high resolution) and includes multispectral bands. The increase in the resolution of satellite images gives us the opportunity to identify actual cultivated areas and

separating them from the neighboring land-cover components. While the increase in the number of spectral bands provide the opportunity to differentiate between land cover components more accurately because the difference in band wavelengths cause different interaction with the land components.

In this paper, the above two preferable image characteristics were achieved; i.e. the image resolution has been achieved by enlarging the image size, using a hybrid technique including DWT and SWT methods, while the multispectral bands establishment was achieved by implementing the histogram specification (or matching) method. The results showed that the created image bands provided better estimation of the cultivated areas when compared with the actual areas of the rice cultured farms as published by the Iraqi Ministry of Agriculture, using both the normalized difference vegetation index (NDVI) and scatterplot classification methods (SCP). What is remain to note is that; differences between the estimated and the actual agriculture areas may be due to the inaccurate values published by the Iraqi Ministry of Agriculture.

References

[1] S.M. Ali, and S.S. Salman, "Estimating the Yield of Rice Farms in Southern Iraq using Landsat images," International Journal of Scientific & Engineering Research, Volume 6, Issue 8, pp. 1607-1614, August-2015

[2] S.M. Ali, and S.S. Salman, "Chronological Calibration Methods for Landsat Satellite Images," IOSR Journal of Applied Physics, Volume 7, Issue 6,PP 107-115, Nov. - Dec. 2015.

[3] H. Demirel, and G. Anbarjafari, "Satellite image resolution enhancement using complex wavelet transform," IEEE Geoscience and Remote Sensing Letter, vol. 7, no. 1, pp. 123–126, Jan. 2010

[4] S.M. Ali, " Multi-sensors, Multi-resolution Data Fusion Using Principal Components Analysis and Histogram Specification Techniques," International Journal of Geographical Information System Applications and Remote Sensing, Vol. 1, No. 1, pp. 21-37, July2010

[5] C. Ricotta, G. Avena, and A.D. Palma, "Mapping and monitoring net primary productivity with AVHRRNDVI time-series: statistical equivalence of cumulative vegetation indices," ISPRS journal of photogrammetry and remote sensing, **54**, pp. 325-331, 1999

[6] S.M. Ali, "New Fully Automatic Multispectral Image Classification based on Scatterplot Method," International Journal of Emerging Technology and Advanced Engineering, Volume 3, Issue 10, pp.388-394, October 2013

[7] Mostafa K. Mosleh, Quazi K. Hassan, and Ehsan H. Chowdhury, " Application of remote sensors in mapping rice area and forecasting Its Production: A Review," Sensors, 15, 769-791, 2015

[8] Y. Piao, I. Shin, and H. W. Park, "Image resolution enhancement using inter-subband correlation in wavelet domain," in Proc. Int. Conf. Image Process., 2007, vol. 1, pp. I-445–448.

[9] S. Mallat, A Wavelet Tour of Signal Processing, 2nd ed. New York: Academic, 1999.

[10] J. E. Fowler, "The redundant discrete wavelet transform and additive noise," Mississippi State ERC, Mississippi State University, Tech. Rep.MSSU-COE-ERC-04-04, Mar. 2004.

[11] R.C. Gonzalez, and R.E. Woods, "Digital Image Processing," 2nd ed. (Prentice Hall, Upper Saddle River, New Jersey 07458, 2002)

[12] A. K. Bhandaria , A. Kumara, and G. K. Singhb, "Feature Extraction using Normalized Difference Vegetation Index (NDVI): a Case Study of Jabalpur City," 2nd International Conference on Communication, Computing & Security [ICCCS-2012], Procedia Technology 6, pp. 612 – 621, 2012

[13] Rouse, J.W., R.H. Haas, J.A. Schell, and D.W. Deering, "Monitoring Vegetation Systems in the Great Plains with ERTS," 3rd ERTS Symposium, NASA SP-351 I: pp.309-317. 1973.

[14] Crippen, R.E., "Calculating the vegetation index faster," Remote Sensing of Environment, **34**, pp.71-73, 1990.